Evidence for $\psi/$ Decays into $\gamma\pi^0$ and $\gamma\eta$

M. Ablikim,[1] M. N. Achasov,[5] L. An,[9] Q. An,[35] Z. H. An,[1] J. Z. Bai,[1] R. Baldini,[17] Y. Ban,[22] J. Becker,[2] N. Berger,[1] M. Bertani,[17] J. M. Bian,[1] I. Boyko,[15] R. A. Briere,[3] V. Bytev,[15] X. Cai,[1] G. F. Cao,[1] X. X. Cao,[1] J. F. Chang,[1] G. Chelkov,[15,*] G. Chen,[1] H. S. Chen,[1] J. C. Chen,[1] M. L. Chen,[1] S. J. Chen,[20] Y. Chen,[1] Y. B. Chen,[1] H. P. Cheng,[11] Y. P. Chu,[1] D. Cronin-Hennessy,[34] H. L. Dai,[1] J. P. Dai,[1] D. Dedovich,[15] Z. Y. Deng,[1] I. Denysenko,[15,†] M. Destefanis,[37] Y. Ding,[18] L. Y. Dong,[1] M. Y. Dong,[1] S. X. Du,[41] M. Y. Duan,[25] R. R. Fan,[1] J. Fang,[1] S. S. Fang,[1] F. Feldbauer,[2] C. Q. Feng,[35] C. D. Fu,[1] J. L. Fu,[20] Y. Gao,[31] C. Geng,[35] K. Goetzen,[7] W. X. Gong,[1] M. Greco,[37] S. Grishin,[15] M. H. Gu,[1] Y. T. Gu,[9] Y. H. Guan,[6] A. Q. Guo,[21] L. B. Guo,[19] Y. P. Guo,[21] X. Q. Hao,[1] F. A. Harris,[33] K. L. He,[1] M. He,[1] Z. Y. He,[21] Y. K. Heng,[1] Z. L. Hou,[1] H. M. Hu,[1] J. F. Hu,[6] T. Hu,[1] B. Huang,[1] G. M. Huang,[12] J. S. Huang,[10] X. T. Huang,[24] Y. P. Huang,[1] T. Hussain,[36] C. S. Ji,[35] Q. Ji,[1] X. B. Ji,[1] X. L. Ji,[1] L. K. Jia,[1] L. L. Jiang,[1] X. S. Jiang,[1] J. B. Jiao,[24] Z. Jiao,[11] D. P. Jin,[1] S. Jin,[1] F. F. Jing,[31] M. Kavatsyuk,[16] S. Komamiya,[30] W. Kuehn,[32] J. S. Lange,[32] J. K. C. Leung,[29] Cheng Li,[35] Cui Li,[35] D. M. Li,[41] F. Li,[1] G. Li,[1] H. B. Li,[1] J. C. Li,[1] Lei Li,[1] N. B. Li,[19] Q. J. Li,[1] W. D. Li,[1] W. G. Li,[1] X. L. Li,[24] X. N. Li,[1] X. Q. Li,[21] X. R. Li,[1] Z. B. Li,[27] H. Liang,[35] Y. F. Liang,[26] Y. T. Liang,[32] G. R. Liao,[8] X. T. Liao,[1] B. J. Liu,[28] B. J. Liu,[29] C. L. Liu,[3] C. X. Liu,[1] C. Y. Liu,[1] F. H. Liu,[25] Fang Liu,[1] Feng Liu,[12] G. C. Liu,[1] H. Liu,[1] H. B. Liu,[6] H. M. Liu,[1] H. W. Liu,[1] J. P. Liu,[39] K. Liu,[22] K. Y. Liu,[18] Q. Liu,[33] S. B. Liu,[35] X. H. Liu,[1] Y. B. Liu,[21] Y. W. Liu,[35] Yong Liu,[1] Z. A. Liu,[1] Z. Q. Liu,[1] H. Loehner,[16] G. R. Lu,[10] H. J. Lu,[11] J. G. Lu,[1] Q. W. Lu,[25] X. R. Lu,[6] Y. P. Lu,[1] C. L. Luo,[19] M. X. Luo,[40] T. Luo,[1] X. L. Luo,[1] C. L. Ma,[6] F. C. Ma,[18] H. L. Ma,[1] Q. M. Ma,[1] T. Ma,[1] X. Ma,[1] X. Y. Ma,[1] M. Maggiora,[37] Q. A. Malik,[36] H. Mao,[1] Y. J. Mao,[22] Z. P. Mao,[1] J. G. Messchendorp,[16] J. Min,[1] R. E. Mitchell,[14] X. H. Mo,[1] C. Motzko,[2] N. Yu. Muchnoi,[5] Y. Nefedov,[15] Z. Ning,[1] S. L. Olsen,[23] Q. Ouyang,[1] S. Pacetti,[17] M. Pelizaeus,[33] K. Peters,[7] J. L. Ping,[19] R. G. Ping,[1] R. Poling,[34] C. S. J. Pun,[29] M. Qi,[20] S. Qian,[1] C. F. Qiao,[6] X. S. Qin,[1] J. F. Qiu,[1] K. H. Rashid,[36] G. Rong,[1] X. D. Ruan,[9] A. Sarantsev,[15,‡] J. Schulze,[2] M. Shao,[35] C. P. Shen,[33] X. Y. Shen,[1] H. Y. Sheng,[1] M. R. Shepherd,[14] X. Y. Song,[1] S. Sonoda,[30] S. Spataro,[37] B. Spruck,[32] D. H. Sun,[1] G. X. Sun,[1] J. F. Sun,[10] S. S. Sun,[1] X. D. Sun,[1] Y. J. Sun,[35] Y. Z. Sun,[1] Z. J. Sun,[1] Z. T. Sun,[35] C. J. Tang,[26] X. Tang,[1] X. F. Tang,[8] H. L. Tian,[1] D. Toth,[34] G. S. Varner,[33] X. Wan,[1] B. Q. Wang,[22] K. Wang,[1] L. L. Wang,[4] L. S. Wang,[1] P. Wang,[1] P. L. Wang,[1] Q. Wang,[1] S. G. Wang,[22] X. L. Wang,[35] Y. D. Wang,[35] Y. F. Wang,[1] Y. Q. Wang,[24] Z. Wang,[1] Z. G. Wang,[1] Z. Y. Wang,[1] D. H. Wei,[8] S. P. Wen,[1] U. Wiedner,[2] L. H. Wu,[1] N. Wu,[1] W. Wu,[18] Z. Wu,[1] Z. J. Xiao,[19] Y. G. Xie,[1] G. F. Xu,[1] G. M. Xu,[22] H. Xu,[1] Y. Xu,[21] Z. R. Xu,[35] Z. Z. Xu,[35] Z. Xue,[1] L. Yan,[35] W. B. Yan,[35] Y. H. Yan,[13] H. X. Yang,[1] M. Yang,[1] T. Yang,[9] Y. Yang,[12] Y. X. Yang,[8] M. Ye,[1] M. H. Ye,[4] B. X. Yu,[1] C. X. Yu,[21] L. Yu,[12] C. Z. Yuan,[1] W. L. Yuan,[19] Y. Yuan,[1] A. A. Zafar,[36] A. Zallo,[17] Y. Zeng,[13] B. X. Zhang,[1] B. Y. Zhang,[1] C. C. Zhang,[1] D. H. Zhang,[1] H. H. Zhang,[27] H. Y. Zhang,[1] J. Zhang,[19] J. W. Zhang,[1] J. Y. Zhang,[1] J. Z. Zhang,[1] L. Zhang,[20] S. H. Zhang,[1] T. R. Zhang,[19] X. J. Zhang,[1] X. Y. Zhang,[24] Y. Zhang,[1] Y. H. Zhang,[1] Z. P. Zhang,[35] Z. Y. Zhang,[39] G. Zhao,[1] H. S. Zhao,[1] Jiawei Zhao,[35] Jingwei Zhao,[1] Lei Zhao,[35] Ling Zhao,[1] M. G. Zhao,[21] Q. Zhao,[1] S. J. Zhao,[41] T. C. Zhao,[38] X. H. Zhao,[20] Y. B. Zhao,[1] Z. G. Zhao,[35] Z. L. Zhao,[9] A. Zhemchugov,[15,*] B. Zheng,[1] J. P. Zheng,[1] Y. H. Zheng,[6] Z. P. Zheng,[1] B. Zhong,[1] J. Zhong,[2] L. Zhong,[31] L. Zhou,[1] X. K. Zhou,[6] X. R. Zhou,[35] C. Zhu,[1] K. Zhu,[1] K. J. Zhu,[1] S. H. Zhu,[1] X. L. Zhu,[31] X. W. Zhu,[1] Y. S. Zhu,[1] Z. A. Zhu,[1] J. Zhuang,[1] B. S. Zou,[1] J. H. Zou,[1] J. X. Zuo,[1] and P. Zweber[34]

(BESIII Collaboration)

[1]*Institute of High Energy Physics, Beijing 100049, People's Republic of China*
[2]*Bochum Ruhr-University, 44780 Bochum, Germany*
[3]*Carnegie Mellon University, Pittsburgh, Pennsylvania 15213, USA*
[4]*China Center of Advanced Science and Technology, Beijing 100190, People's Republic of China*
[5]*G.I. Budker Institute of Nuclear Physics SB RAS (BINP), Novosibirsk 630090, Russia*
[6]*Graduate University of Chinese Academy of Sciences, Beijing 100049, People's Republic of China*
[7]*GSI Helmholtzcentre for Heavy Ion Research GmbH, D-64291 Darmstadt, Germany*
[8]*Guangxi Normal University, Guilin 541004, People's Republic of China*
[9]*Guangxi University, Naning 530004, People's Republic of China*
[10]*Henan Normal University, Xinxiang 453007, People's Republic of China*
[11]*Huangshan College, Huangshan 245000, People's Republic of China*
[12]*Huazhong Normal University, Wuhan 430079, People's Republic of China*
[13]*Hunan University, Changsha 410082, People's Republic of China*
[14]*Indiana University, Bloomington, Indiana 47405, USA*

[15]Joint Institute for Nuclear Research, 141980 Dubna, Russia
[16]KVI/University of Groningen, 9747 AA Groningen, The Netherlands
[17]Laboratori Nazionali di Frascati - INFN, 00044 Frascati, Italy
[18]Liaoning University, Shenyang 110036, People's Republic of China
[19]Nanjing Normal University, Nanjing 210046, People's Republic of China
[20]Nanjing University, Nanjing 210093, People's Republic of China
[21]Nankai University, Tianjin 300071, People's Republic of China
[22]Peking University, Beijing 100871, People's Republic of China
[23]Seoul National University, Seoul, 151-747 Korea
[24]Shandong University, Jinan 250100, People's Republic of China
[25]Shanxi University, Taiyuan 030006, People's Republic of China
[26]Sichuan University, Chengdu 610064, People's Republic of China
[27]Sun Yat-Sen University, Guangzhou 510275, People's Republic of China
[28]The Chinese University of Hong Kong, Shatin, N.T., Hong Kong.
[29]The University of Hong Kong, Pokfulam, Hong Kong
[30]The University of Tokyo, Tokyo 113-0033 Japan
[31]Tsinghua University, Beijing 100084, People's Republic of China
[32]Universitaet Giessen, 35392 Giessen, Germany
[33]University of Hawaii, Honolulu, Hawaii 96822, USA
[34]University of Minnesota, Minneapolis, Minnesota 55455, USA
[35]University of Science and Technology of China, Hefei 230026, People's Republic of China
[36]University of the Punjab, Lahore-54590, Pakistan
[37]University of Turin and INFN, Turin, Italy
[38]University of Washington, Seattle, Washington 98195, USA
[39]Wuhan University, Wuhan 430072, People's Republic of China
[40]Zhejiang University, Hangzhou 310027, People's Republic of China
[41]Zhengzhou University, Zhengzhou 450001, People's Republic of China

(Received 4 November 2010; published 20 December 2010)

The decays $\psi' \to \gamma\pi^0$, $\gamma\eta$ and $\gamma\eta'$ are studied using data collected with the BESIII detector at the BEPCII e^+e^- collider. The processes $\psi' \to \gamma\pi^0$ and $\psi' \to \gamma\eta$ are observed for the first time with signal significances of 4.6σ and 4.3σ, respectively. The branching fractions are determined to be $\mathcal{B}(\psi' \to \gamma\pi^0) = (1.58 \pm 0.40 \pm 0.13) \times 10^{-6}$, $\mathcal{B}(\psi' \to \gamma\eta) = (1.38 \pm 0.48 \pm 0.09) \times 10^{-6}$, and $\mathcal{B}(\psi' \to \gamma\eta') = (126 \pm 3 \pm 8) \times 10^{-6}$, where the first errors are statistical and the second ones systematic.

DOI: 10.1103/PhysRevLett.105.261801 PACS numbers: 13.20.Gd

The study of vector charmonium radiative decay to a neutral pseudoscalar meson $P = (\pi^0, \eta, \eta')$ provides important tests for various phenomenological mechanisms, such as the vector meson dominance model (VDM) [1–3], two-gluon couplings to $q\bar{q}$ states [2], mixing of $\eta_c - \eta^{(\prime)}$ [4,5], and final-state radiation by light quarks [1]. Direct contributions from the continuum through a virtual photon $e^+e^- \to \gamma^* \to \gamma P$ are relevant to the decays of J/ψ, ψ' and ψ'' to γP as discussed recently in Ref. [6]. Furthermore, the possible interference between the charmonium decays and continuum process may play a key role in understanding the difference between J/ψ and ψ' decays into γP [7].

For $P = \eta$ and η', the ratio $R_{J/\psi} \equiv \mathcal{B}(J/\psi \to \gamma\eta)/\mathcal{B}(J/\psi \to \gamma\eta')$ can be predicted by first order perturbation theory [1]. The analogous ratio ($R_{\psi'}$) can be defined for ψ' radiative decays into η and η', and $R_{\psi'} \approx R_{J/\psi}$ is expected [8]. Recently, the CLEO Collaboration reported measurements for the decays of J/ψ, ψ' and ψ'' to γP [8], and no evidence for $\psi' \to \gamma\eta$ or $\gamma\pi^0$ was found. Therefore they obtain $R_{\psi'} \ll R_{J/\psi}$ with $R_{\psi'} < 1.8\%$ at the 90% C.L. and $R_{J/\psi} = (21.1 \pm 0.9)\%$ [8]. Such a small $R_{\psi'}$ is unanticipated, and it poses a significant challenge to our understanding of the $c\bar{c}$ bound states.

The decay $\psi' \to \gamma\pi^0$ is suppressed in QED because the photon can only be produced from final-state radiation off one of the quarks. It has also been described via the strong process $\psi' \to ggg \to \rho^*\pi^0$, $\rho^* \to \gamma$ in the VDM [3]. In Ref. [6], the contribution from $\psi' \to \gamma^* \to \gamma\pi^0$ is calculated, and $\mathcal{B}(\psi' \to \gamma\pi^0) \approx 2.19 \times 10^{-7}$ is obtained, which is compatible to the VDM contribution and does not contradict the upper limit of 5.0×10^{-6} (at the 90% C.L.) reported by the CLEO Collaboration [8]. The $\gamma^* - \gamma - \pi^0$ vertex was shown [9] to be characterized by a form factor $F(Q^2)$, where $Q^2 \equiv -q^2$ and q is the four-momentum of the virtual photon γ^*. By using $e^+e^- \to e^+e^-\pi^0$, the form factor was measured in the CLEO [10] and *BABAR* [11] experiments for spacelike nonasymptonic momentum transfer in the range $|q^2| = 1.6$–8.0 GeV^2 and 4–40 GeV^2, respectively. The $e^+e^- \to \psi'/\gamma^* \to \gamma\pi^0$ process will be very useful in testing the form factor for timelike photons $Q^2 = -q^2 < 0$ [6].

In this Letter, $\psi' \to \gamma\pi^0$ is studied using $\pi^0 \to \gamma\gamma$ decay, $\psi' \to \gamma\eta$ is measured using $\eta \to \pi^+\pi^-\pi^0$ and $\eta \to \pi^0\pi^0\pi^0$ with $\pi^0 \to \gamma\gamma$, and $\psi' \to \gamma\eta'$ is studied using $\eta' \to \gamma\pi^+\pi^-$ and $\eta' \to \pi^+\pi^-\eta$ with $\eta \to \gamma\gamma$. The analyses use a data sample of 156.4 pb^{-1} collected at the ψ' peak with the BESIII detector operating at BEPCII [12,13]. By measuring the production of multihadronic events, the number of ψ' decays is found to be $(1.06 \pm 0.04) \times 10^8$ [14]. An independent data sample of 42.6 pb^{-1} taken at $\sqrt{s} = 3.65$ GeV is utilized to determine the potential background contribution from the continuum.

BEPCII is a double-ring e^+e^- collider designed to provide e^+e^- beams with a peak luminosity of 10^{33} cm^{-2} s^{-1} at a beam current of 0.93 A. The cylindrical core of the BESIII detector consists of a helium-based main drift chamber (MDC), a plastic scintillator time-of-flight system (TOF), and a CsI(Tl) electromagnetic calorimeter (EMC), which are all enclosed in a superconducting solenoidal magnet providing a 1.0 T magnetic field. The solenoid is supported by an octagonal flux-return yoke with resistive plate counter muon identifier modules interleaved with steel. The acceptance of charged particles and photons is 93% over 4π stereo angle, and the charged-particle momentum and photon energy resolutions at 1 GeV are 0.5% and 2.5%, respectively.

The BESIII detector is modeled with a Monte Carlo (MC) simulation based on GEANT4 [15,16]. EVTGEN [17] is used to generate $\psi' \to \gamma\pi^0$, $\gamma\eta$, $\gamma\eta'$ events, where the angular distribution of the radiative photon from ψ' decay is $1 + \cos^2\theta$ in the ψ' frame. The decay $\eta \to \pi^+\pi^-\pi^0$ is generated according to the Dalitz distribution measured in [18] and $\eta' \to \gamma\pi^+\pi^-$ is simulated assuming it is mediated by $\rho^0 \to \pi^+\pi^-$, while the decays of $\eta \to \pi^0\pi^0\pi^0$ and $\eta' \to \pi^+\pi^-\eta$ are generated with phase space. ψ' decays are simulated by the MC event generator KKMC [19] with known decays modeled by the EVTGEN according to the branching fractions provided by the Particle Data Group (PDG) [20], and the remaining unknown decay modes generated with LUNDCHARM [17].

Charged tracks in BESIII are reconstructed using MDC hits. To optimize the momentum measurement, we select tracks in the polar angle range $|\cos\theta| < 0.93$ and require that they pass within ± 10 cm from the Interaction Point (IP) in the beam direction and within ± 1 cm of the beam line in the plane perpendicular to the beam. All the charged tracks are assumed to be pions, and particle identification (PID) is not required, except in $\eta' \to \gamma\rho$ where the dE/dx information has been used to suppress QED background, most of which is from $e^+e^- \to e^+e^-\gamma$. Either zero or two tracks with net charge zero are required for the final $\pi^0/\eta/\eta'$ decay products.

Electromagnetic showers are reconstructed by clustering EMC crystal energies. The energy deposited in nearby TOF counters is included to improve the reconstruction efficiency and energy resolution. Showers identified as photon candidates must satisfy fiducial and shower-quality requirements. For the $\psi' \to \gamma\eta$ and $\gamma\eta'$ analyses, the photon candidate showers are reconstructed from both the barrel and end cap of the EMC, and showers from barrel region ($|\cos\theta| < 0.8$) must have a minimum energy of 25 MeV, while those in the end caps ($0.86 < |\cos\theta| < 0.92$) must have at least 50 MeV. The showers in the angular range between the barrel and end cap are poorly reconstructed and excluded from the analyses. To exclude showers from charged particles, a photon must be separated by at least 10° from any charged track. The EMC cluster timing requirements are used to suppress electronic noise and energy deposits unrelated to the event.

Events with the decay modes shown in Table I are selected. Every particle in the final state must be explicitly found, and their vertex must be consistent with the measured beam spot. The sum of four-momenta of all particles is constrained to the known ψ' mass [20] and initial e^+e^- three-momentum in the lab frame. The vertex and full event four-momentum kinematic fits must satisfy $\chi^2_{Vx} < 100$ and $\chi^2_{4C} < 40$, respectively. For $\eta \to 3\pi^0$, a looser restriction of $\chi^2_{4C} < 90$ is applied to increase efficiency. Further selections are based on four-momenta from the kinematic fit. In η/η' channels, photon pairs are used to reconstruct π^0 or η candidates if their invariant mass satisfies $M_{\gamma\gamma} \in (120, 150)$ MeV/c^2 or $(515, 565)$ MeV/c^2, respectively.

For the $\psi' \to \gamma\pi^0$ analysis, the primary background comes from the continuum process $e^+e^- \to \gamma\gamma(\gamma)$, where the two energetic photons are distributed in the forward and backward regions. We require that photon candidate showers lie in the barrel region of the EMC to suppress this background. Since π^0 mesons decay isotropically, the angular distribution of photons from π^0 decays is flat in the π^0 helicity frame. However, continuum background events accumulate near $\cos\theta_{\rm decay} = \pm 1$, where $\theta_{\rm decay}$ is the angle of the decay photon in the π^0 helicity frame [14]. To further suppress continuum background, we require $|\cos\theta_{\rm decay}| < 0.5$. Another potentially serious background comes from $e^+e^- \to \gamma\gamma$, in which one γ converts into an

TABLE I. For each decay mode, the number of signal events (N_S), the number of scaled continuum background events (N_C) in the signal region, the number of expected background events from ψ' decays (N_R) in the signal region, and the MC efficiency (ε) for signal are given. The error on N_S is only the statistical error, and the signal region is defined to be within $\pm 3\sigma$ from the nominal π^0, η, and η' masses.

Modes ($\psi' \to \gamma X$)	N_S	N_C	N_R	ϵ(%)
$\psi' \to \gamma\pi^0$	37.4 ± 9.5	63.5	1.8	21.4
$\psi' \to \gamma\eta(\pi^+\pi^-\pi^0)$	8.9 ± 3.6	2.2	0.0	21.0
$\psi' \to \gamma\eta(\pi^0\pi^0\pi^0)$	3.8 ± 2.3	0.0	1.2	10.7
$\psi' \to \gamma\eta'[\pi^+\pi^-\eta(\gamma\gamma)]$	586 ± 25	0.0	4.7	27.1
$\psi' \to \gamma\eta'(\pi^+\pi^-\gamma)$	1640 ± 44	179.3	111.7	41.0

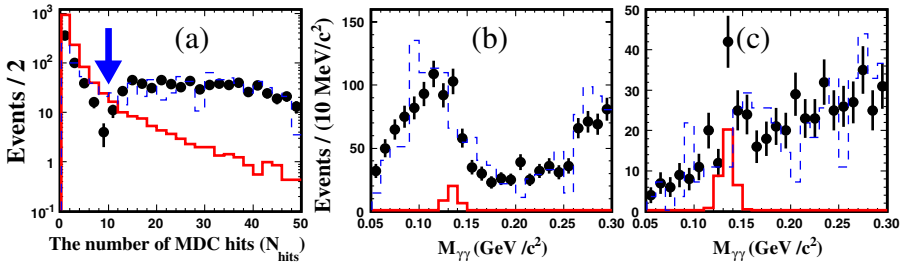

FIG. 1 (color online). The distribution of (a) the number of MDC hits, and the two-photon invariant mass distributions for $\gamma\pi^0$ final states (b) without and (c) with the $N_{\rm hits} \leq 10$ requirement. Solid histograms are the MC-simulated signal for $\psi' \to \gamma\pi^0$, dashed histograms are the luminosity scaled continuum data, and points are ψ' data. The solid arrow indicates the requirement on $N_{\rm hits}$.

e^+e^- pair in the outer part of the MDC. If the track finding algorithm fails to find the track, the two showers in the EMC are identified as isolated photons without associated charged tracks. To suppress this background, the number of MDC hits, $N_{\rm hits}$, is counted in the sector between the two radial lines connecting the IP and the two-shower positions in the EMC. To take the EMC spacial resolution into account, the sector is extended by 3.5° on both sides. Because of high beam related background level, the hits in the inner 8 MDC layers are not counted in $N_{\rm hits}$. Figure 1(a) shows the $N_{\rm hits}$ distribution. As shown in Fig. 1(b), background from continuum event γ conversions $e^+e^- \to \gamma\gamma$ accumulates in the low mass region. After requiring $N_{\rm hits} \leq 10$, this background is reduced dramatically, while there is still an accumulation of events at the π^0 mass, as shown in Fig. 1(c).

After applying the above selection criteria, the mass spectra of π^0, η, and η' candidates are shown in Fig. 2. An unbinned maximum likelihood (ML) fit is used for each analysis to determine the event yields except for $\psi' \to \gamma\eta(\pi^0\pi^0\pi^0)$. The signal probability density function (PDF) in each mode is obtained from MC simulation. The shape for the continuum background is described by a second order Chebychev polynomial function, and the yield and its PDF parameters are floated in the fit. The fitting ranges for π^0, η and η' are 0.05–0.30 GeV/c^2, 0.40–0.70 GeV/c^2, and 0.85–1.05 GeV/c^2, respectively. The signal yield for $\psi' \to \gamma\eta(\pi^0\pi^0\pi^0)$ is determined directly by counting the number of events in the signal region, which is in 0.51–0.57 GeV/c^2, about 3 standard deviations from the nominal value of the η mass [20] as shown in Fig. 2(c), while the sideband regions are defined as 0.42–0.48 GeV/c^2 and 0.60–0.66 GeV/c^2. The signal yields and the efficiencies are summarized in Table I.

The backgrounds remaining after event selection can be divided into two categories. One is from ψ' decays, which can be studied using a sample of 10^8 MC-simulated inclusive ψ' events. The other is from nonresonant processes or initial state radiation to low mass resonances, which can be studied using the continuum data sample collected at a center of mass energy of 3.65 GeV. The expected backgrounds from ψ' decays are listed in Table I, where the number of background events is the number in the signal region, which is defined as within $\pm 3\sigma$ from the nominal π^0, η and η' masses. For $\psi' \to \gamma\pi^0$, the normalized number of events from $\psi' \to \gamma\pi^0\pi^0$ is 1.8 in the π^0 signal range. For $\psi' \to \gamma\eta(\pi^0\pi^0\pi^0)$, there are 1.2 events from the decay of $\psi' \to \gamma\eta(\gamma\gamma)\eta(3\pi^0)$. For $\psi' \to \gamma\eta'(\gamma\pi^+\pi^-)$, the main background from ψ' decays is $\psi' \to \rho^0\pi^0$ which contributes a smooth background. The QED backgrounds for $\psi' \to \gamma\eta'(\pi^+\pi^-\gamma)$ are from $e^+e^- \to \gamma\mu^+\mu^-$ and $e^+e^- \to \gamma e^+e^-$, and both of them give a smooth background under the η' signal peak. For $\psi' \to \gamma\pi^0$, a smooth background is contributed from $e^+e^- \to \gamma\gamma(\gamma)$ events. The cross section for $e^+e^- \to \gamma^* \to \gamma\pi^0(\gamma\eta)$ has been estimated using data collected

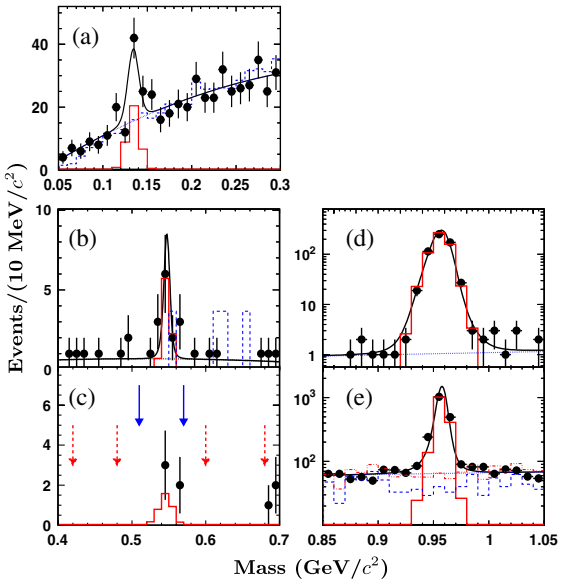

FIG. 2 (color online). Mass distributions of the pseudoscalar meson candidates in $\psi' \to \gamma P$: (a) $\gamma\pi^0$, (b) $\gamma\eta(\pi^+\pi^-\pi^0)$, (c) $\gamma\eta(3\pi^0)$, (d) $\gamma\eta'[\pi^+\pi^-\eta(\gamma\gamma)]$, and (e) $\gamma\eta'(\gamma\pi^+\pi^-)$. The crosses are data, the solid histograms are the MC-simulated signal, and the dashed lines are the continuum backgrounds. Fits are shown as solid lines, background polynomials as dotted lines. In (c), the arrows indicate nominal selection criteria, while the dashed arrows show sidebands. In (e), the dot-dot-dashed line shows the sum of the continuum background and the expected background from ψ' decays.

TABLE II. Summary of systematic errors (%).

Sources	π^0	$\eta \to \pi^+\pi^-\pi^0$	$\eta \to 3\pi^0$	$\eta' \to \pi^+\pi^-\eta(\gamma\gamma)$	$\eta' \to \pi^+\pi^-\gamma$
MDC track finding	...	4	...	4	4
Photon detection	2	2	6	2	1
$\pi^0(\eta)$ reconstruction	...	1	3	1	...
4C kinematic fit	1	3	0	3	2
Background shape	4.8	6.4	...	0	1
Number of ψ'	4	4	4	4	4
Cited branching fractions	0	1.2	0.7	1.7	1.7
MDC hits	3	...	...	...	...
Number of photons	4	...	...	...	...
Total	8.3	9.4	7.8	7.0	6.4

at $\sqrt{s} = 3.65$ GeV, and the upper limit on the cross section is less than 0.14(0.68) pb at the 90% C.L. Since the continuum cross section is small, we neglect possible interference between $\psi' \to \gamma\pi^0(\eta)$ signal and continuum $\gamma\pi^0(\eta)$. All the backgrounds are summarized in Table I.

The systematic uncertainties for these measurements are summarized in Table II. The uncertainties due to MDC track finding and photon detection are 2% per charged track and 1% per low energy photon. The uncertainty of detecting the high energy photon is less than 0.25% which can be neglected. The systematic errors from π^0 (η) reconstruction is determined to be 1% per π^0 (η) by using a high purity control sample of $J/\psi \to \pi^0\bar{p}p$ ($J/\psi \to \eta\bar{p}p$) decay. The uncertainties due to kinematic fits have been estimated using the control samples with the same event topologies as those in the signal cases, i.e., the same number of charged tracks and same number of photons. The systematic uncertainties due to the dE/dx requirements to identify charged pions in the $\psi' \to \gamma\eta'(\gamma\pi^+\pi^-)$ and N_γ in the $\psi' \to \gamma\pi^0$ are studied by using the control samples of $J/\psi \to \rho\pi$ and $J/\psi \to \gamma\eta(\gamma\gamma)$, respectively, with and without applying these requirements.

In $\psi' \to \gamma\pi^0$, the uncertainty due to the requirement on the MDC hits, $N_{\rm hits} \leq 10$, is studied using a sample of $J/\psi \to \gamma\eta$, $\eta \to \gamma\gamma$ events. The ratios of events with and without the requirement on the number of MDC hits are obtained for both data and MC simulation. Taking the difference of opening angle between $J/\psi \to \gamma\eta(\gamma\gamma)$ and $\psi' \to \gamma\pi^0$ into account, the difference 3% is considered as the systematic error for the measurement of $\psi' \to \gamma\pi^0$ and is due to the difference in the noise in the MDC for data and MC simulation.

The uncertainty due to the background shape has been estimated by varying the PDF shape and fitting range in the ML fit. For the intermediate decays, the $\eta(\eta')$ branching fractions and uncertainties from the PDG fit [20] are used. The total relative systematic errors on these measurements are 8.3%, 9.4%, 7.8%, 7.0%, and 6.4% for $\psi' \to \gamma\pi^0$, $\psi' \to \gamma\eta(\pi^+\pi^-\pi^0)$, $\psi' \to \gamma\eta(\pi^0\pi^0\pi^0)$, $\psi' \to \gamma\eta'[\pi^+\pi^-\eta(\gamma\gamma)]$, and $\psi' \to \gamma\eta'(\pi^+\pi^-\gamma)$, respectively, as summarized in Table II.

The branching fractions of ψ' decays to γ and a pseudoscalar meson are listed in Table III. Taking the common systematic errors into account, the combined measurements for $\psi' \to \gamma\eta$, $\gamma\eta'$ modes are obtained. The PDG [20] values are also shown in Table III. With considering the background shape uncertainty, we find the signal significance for $\psi' \to \gamma\pi^0(\gamma\eta)$ to be $4.6(4.3)\sigma$, as determined by the ratio of the maximum likelihood value and the likelihood value for a fit where the signal contribution is set to zero.

In summary, we have measured branching fractions for $\psi' \to \gamma\pi^0$, $\psi' \to \gamma\eta$ and $\psi' \to \gamma\eta'$ decays. For the first time, we find evidence for the $\psi' \to \gamma\pi^0$ and $\psi' \to \gamma\eta$ decays with signal significances of 4.6σ and 4.3σ, respectively. The evidence for $\psi' \to \gamma\pi^0$ will yield an experimental constraint on the $\gamma^* \to \gamma\pi^0$ vertex in the timelike regime at $|q^2| = m^2_{\psi'}$ [6]. For the ratio of η and η' production rates from ψ' decays, we obtain $R_{\psi'} = (1.10 \pm 0.38 \pm 0.07)\%$, where the statistical and systematic uncertainties from the input branching fractions as listed in

TABLE III. Branching fractions (10^{-6}) from this analysis, where the first errors are statistical and the second ones are systematic, and the comparison with the PDG values [20].

Mode	BESIII	Combined BESIII	PDG
$\psi' \to \gamma\pi^0$	$1.58 \pm 0.40 \pm 0.13$	$1.58 \pm 0.40 \pm 0.13$	≤ 5
$\psi' \to \gamma\eta(\pi^+\pi^-\pi^0)$	$1.78 \pm 0.72 \pm 0.17$	$1.38 \pm 0.48 \pm 0.09$	≤ 2
$\to \gamma\eta(\pi^0\pi^0\pi^0)$	$1.07 \pm 0.65 \pm 0.08$		
$\psi' \to \gamma\eta'(\pi^+\pi^-\eta)$	$120 \pm 5 \pm 8$	$126 \pm 3 \pm 8$	121 ± 8
$\to \gamma\eta'(\pi^+\pi^-\gamma)$	$129 \pm 3 \pm 8$		

Table III have been combined in quadrature after accounting for common systematic errors. This ratio is the first measurement, and it is below the 90% C.L. upper bound determined by the CLEO Collaboration [8]. The corresponding $\eta - \eta'$ production ratio for the J/ψ resonance was measured to be $R_{J/\psi} = (21.1 \pm 0.9)\%$ [8]. $R_{\psi'}$ is smaller than $R_{J/\psi}$ by an order of magnitude.

We thank the accelerator group and computer staff of IHEP for their effort in producing beams and processing data. We are grateful for support from our institutes and universities and from these agencies: Ministry of Science and Technology of China, National Natural Science Foundation of China, Chinese Academy of Sciences, Istituto Nazionale di Fisica Nucleare, Russian Foundation for Basic Research, Russian Academy of Science (Siberian branch), U.S. Department of Energy, and National Research Foundation of Korea.

*Also at the Moscow Institute of Physics and Technology, Moscow, Russia.

†On leave from the Bogolyubov Institute for Theoretical Physics, Kiev, Ukraine.

‡Also at the PNPI, Gatchina, Russia.

[1] V. L. Chernyak and A. R. Zhitnitsky, Phys. Rep. **112**, 173 (1984).
[2] J. G. Körner *et al.*, Nucl. Phys. **B229**, 115 (1983).
[3] G. W. Intemann, Phys. Rev. D **27**, 2755 (1983).
[4] H. Fritzsch and J. D. Jackson, Phys. Lett. B **66**, 365 (1977).
[5] K. T. Chao, Nucl. Phys. **B335**, 101 (1990).
[6] J. L. Rosner, Phys. Rev. D **79**, 097301 (2009).
[7] P. Wang *et al.*, Phys. Lett. B **593**, 89 (2004).
[8] T. K. Pedlar *et al.* (CLEO Collaboration), Phys. Rev. D **79**, 111101 (2009).
[9] G. P. Lepage and S. J. Brodsky, Phys. Rev. D **22**, 2157 (1980); S. J. Brodsky and G. P. Lepage, Phys. Rev. D **24**, 1808 (1981).
[10] J. Gronberg *et al.* (CLEO Collaboration), Phys. Rev. D **57**, 33 (1998).
[11] B. Aubert *et al.* (*BABAR* Collaboration), Phys. Rev. D **80**, 052002 (2009).
[12] M. Ablikim *et al.* (BES Collaboration), Nucl. Instrum. Methods Phys. Res., Sect. A **614**, 345 (2010).
[13] "Physics at BES-III", edited by K. T. Chao and Y. Wang [Int. J. Mod. Phys. A **24**, Suppl. 1, 3 (2009)].
[14] M. Ablikim *et al.* (BES Collaboration), Phys. Rev. D **81**, 052005 (2010).
[15] S. Agostinelli *et al.* (GEANT4 Collaboration), Nucl. Instrum. Methods Phys. Res., Sect. A **506**, 250 (2003).
[16] J. Allison *et al.*, IEEE Trans. Nucl. Sci. **53**, 270 (2006).
[17] R. G. Ping, Chinese Phys. C **32**, 599 (2008).
[18] J. G. Layter *et al.*, Phys. Rev. D **7**, 2565 (1973).
[19] S. Jadach, B. F. L. Ward, and Z. Was, Comput. Phys. Commun. **130**, 260 (2000); Phys. Rev. D **63**, 113009 (2001).
[20] K. Nakamura *et al.* (Particle Data Group), J. Phys. G **37**, 075021 (2010).